Radiometric Information Content for Water Vapor and Temperature Profiling in Clear Skies Between 10 and 200 GHz

Swaroop Sahoo, Xavier Bosch-Lluis, Steven C. Reising, *Senior Member, IEEE*, and Jothiram Vivekanandan, *Senior Member, IEEE*

***Abstract*—Atmospheric profiles of water vapor and temperature can be estimated using appropriate retrieval algorithms based on radiometric measurements and atmospheric statistics. Radiometric measurements at multiple frequencies contribute information to profile retrieval, although at some frequencies the information they provide can be highly correlated with that at other frequencies due to similar sensitivities to changes in atmospheric pressure, temperature, and water vapor mixing ratio as a function of altitude. The goal for profile retrieval is to obtain as many independent measurements as possible, both to maximize the vertical resolution and to minimize the retrieval error of the profile. The goal of this study is to determine sets of frequencies in the range from 10 to 200 GHz that provide the largest amount of mutually independent information on water vapor and temperature profiles from ground and airborne instruments for clear sky measurements. Results of such a study are important and useful for frequency selection and design of microwave and millimeter-wave radiometers for humidity and temperature profiling. A branch and bound feature selection algorithm has been used to determine sets of frequencies between 10 and 200 GHz that have the greatest number of degrees of freedom (DOF) for water vapor and temperature retrieval. In general, it has been found that the frequency ranges of 20–23, 85–90, and 165–200 GHz are useful for water vapor profile retrieval, whereas the frequency ranges of 55–65 and 116–120 GHz are useful for temperature profile retrieval. Finally, an analysis has been performed to determine the impact of measurement uncertainty on the number of DOF of measurement and also on the vertical resolution. It was also found that vertical resolution is directly related to the number of DOF.**

***Index Terms*—Atmospheric measurements, feature selection, humidity, radiometry, remote sensing, temperature.**

I. Introduction

TYPICALLY, retrieval algorithms use frequencies near water vapor absorption at 22.235 and 183.31 GHz [1], [2] for humidity profile retrieval as well as frequencies near 60 GHz for temperature profile retrieval [3]. These frequency ranges provide the largest amount of information on water vapor and temperature in the troposphere as a function of altitude. However, accurately determining sets of frequencies that provide the maximum amount of information for retrievals is important to optimize the use of resources when designing and fabricating microwave and millimeter-wave radiometers.

Previous research has focused on information content analysis of the frequency range of 20–70 GHz using eigenvalue analysis of the weighting function (WF) covariance matrix [4]. The WF or Jacobian is the sensitivity of ground-based zenith-viewing brightness temperatures to change in the atmospheric parameter of interest, as shown in (1) and (2) for the parameters of water vapor and temperature, respectively, [5]

$$WF_{\rho_v}(s) = e^{-\tau(0,s)}\frac{\partial\alpha(s)}{\partial\rho_v}\left[T'(s) - T_{b0}e^{-\tau(s,\infty)} - \int_s^\infty T'(s')\alpha e^{-\tau(s,s')}ds'\right] \quad (1)$$

$$WF_T(s) = \frac{dT'}{dT}\alpha(s)e^{-\tau(0,s)} + e^{-\tau(0,s)}\frac{\partial\alpha(s)}{\partial T} \times \left[T'(s) - T_{b0}e^{-\tau(s,\infty)} - \int_s^\infty T'(s')\alpha e^{-\tau(s,s')}ds'\right] \quad (2)$$

where s represents the altitude above ground; $\alpha(s)$ is the total absorption coefficient; $\rho_v(s)$ is the water vapor density; $T(\mathrm{s})$ is the temperature; $T'(s) = \frac{T(s)}{R(T)}$; $R(T) = 1$, where $R(T)$ is the Rayleigh–Jeans approximation factor [6]; T_{b0} is the cosmic background radiation; and $\tau(s_1, s_2)$ is the optical depth from s_1 to s_2, given by $\tau(s_1, s_2) = \int_{s_1}^{s_2}\alpha(s)ds$.

Other previous work has focused on finding the rank of frequencies in 18–37 GHz range to determine those suitable for estimating the wet-path delay using microwave radiometers [7]. This analysis consists of constructing two- and three-frequency sets for 18–37 GHz frequency range. Measurements were simulated for each frequency set using radiosonde data collected from various launch sites, and each set was ranked based on its retrieval noise.

Additionally, the WFs in the frequency range of 10–1000 GHz were analyzed to identify frequencies that are useful in retrieving water vapor and temperature profiles with high vertical resolution from nadir-viewing airborne radiometer measurements [8]. The selected frequency ranges were 43–86 GHz and 121–183 GHz for temperature and water vapor retrieval,

Manuscript received April 10, 2014; revised September 11, 2014; accepted October 09, 2014. Date of publication December 23, 2014; date of current version February 09, 2015. This work was supported in part by the U.S. National Aeronautics and Space Administration, Science Mission Directorate, Earth Science Technology Office, as part of the Instrument Incubator Program under Grant NNX11AH05G and Grant NNX14AK70G.

S. Sahoo, X. Bosch-Lluis, and S. C. Reising are with the Microwave Systems Laboratory, Department of Electrical and Computer Engineering, Colorado State University, Fort Collins, CO 80523 USA (e-mail: swaroop.sahoo@colostate.edu; xavier.bosch-lluis@colostate.edu; steven.reising@colostate.edu).

J. Vivekanandan is with the Earth Observing Laboratory, University Center for Atmospheric Research, Boulder CO 80301 USA (e-mail: vivek@ucar.edu).

Color versions of one or more of the figures in this paper are available online at http://ieeexplore.ieee.org.

Digital Object Identifier 10.1109/JSTARS.2014.2364394

respectively. These frequency sets were found to provide the best resolution for retrieval over the range of effective heights [8] from 1.9 to 6.4 km, although this result varies slightly with season and geographic location. The water vapor and temperature WFs [8] for nadir-viewing radiometers are given in (3) and (4)

$$WF^{\uparrow}_{\rho_v}(s) = e^{-\tau(s,h)}\frac{\partial\alpha(s)}{\partial\rho_v}\left[T'(s) - T^{0\downarrow RE}_{b0}e^{-\tau(0,s)} - \int_0^s T'(s')\alpha e^{-\tau(s',s)}ds'\right] + WF^{\downarrow R}_{\rho_v}(s) \quad (3a)$$

$$T^{0\downarrow RE}_{b0} = (1-r)T'(f,T_S) + (rT_B(f,0,\infty)) \quad (3b)$$

$$WF^{\downarrow R}_{\rho_v}(s) = e^{-\tau(0,s)}rWF_{\rho_v}(s) \quad (3c)$$

$$WF^{\uparrow}_{T}(s) = \frac{dT'}{dT}\alpha(s)e^{-\tau(s,h)} + e^{-\tau(s,h)}\frac{\partial\alpha(s)}{\partial T} \times \left[T'(s) - \int_0^s T'(s')\alpha e^{-\tau(s,s')}ds' - e^{-\tau(0,s)} \times \{(1-r)T' + r(T'(f,T_s) + WF_T(s))\}\right] \quad (4)$$

where

h	observation height above ground level;
r	surface reflection coefficient;
T_S	surface temperature;
$(1-r)T'(f,T_S)$	brightness temperature emitted from the surface;
$T_B(f,0,\infty)$	downwelling brightness temperature;
$(rT_B(f,0,\infty))$	atmospheric downwelling brightness temperature reflected from the surface;
$T^{0\downarrow RE}_{b0}$	sum of the reflected and the emitted radiation; and
WF_{ρ_v} and WF_T	downwelling water vapor and temperature WFs from (1) and (2), respectively.

To extend and expand upon previous work, this paper focuses on determining the maximum number of independent measurements possible in the range from 10 to 200 GHz, with a bandwidth of 100 MHz, for the retrieval of atmospheric water vapor and temperature profiles using zenith-pointing ground-based and nadir-pointing airborne radiometers under a variety of clear sky atmospheric conditions, including winter and summer weather, as well as over the diurnal cycle.

II. Frequency Identification Process Based on Feature Selection to Maximize the Number of Degrees of Freedom

The strategy used in this work is to identify the nonredundant frequencies in the range from 10 to 200 GHz, with a bandwidth of 100 MHz, which contribute to water vapor and temperature profile retrieval, with the goals of fine vertical resolution and good retrieval accuracy. The 100-MHz bandwidth is a requirement to ensure that the frequency channels do not "average over" any features of interest. However, from a practical point of view, radiometers often have bandwidths greater than 100 MHz to reduce noise, but this should not have a significant impact on this study. The number of degrees of freedom (DOF) is used as a criterion and is considered to be the same as the number of independent measurements in the retrieval solution. To determine this number, we first select those frequency sets that are the most sensitive to the atmospheric parameter of interest and retrieve the parameter with optimum vertical resolution from ground level to the top of the troposphere ($\sim$10 km). A feature selection algorithm is used to determine the most significant frequencies by selecting those with linearly independent WFs, i.e., those providing nonredundant information. The WFs are calculated using (1) and (2) for zenith-pointing ground-based radiometers and (3) and (4) nadir-pointing airborne radiometers.

WFs are dependent on atmospheric conditions and on measurement frequency. Therefore, atmospheric parameters are needed to compute the WF for each frequency. These parameters can be obtained from radiosondes that are launched 2–4 times daily from many weather stations in and near populated areas of the world's land masses. This study uses radiosonde data from the U.S. Department of Energy (DOE)'s Atmospheric Radiation Measurement (ARM) Southern Great Plains (SGP) site near Lamont, Oklahoma (OK), USA to calculate the WFs [9].

A. Feature Selection and Number of DOF

Feature selection [10], [11], also known as variable selection, is the process of selection of a subset of relevant variables from a larger set. For this study, the variables are the measurement frequencies. When using a feature selection algorithm, the main assumption is that the data (here the WFs) have some redundant or irrelevant elements and the goal is to identify and remove them. Therefore, feature selection is a dimensionality reduction algorithm. In this study, a branch and bound algorithm [12] is used, as described below.

Assume that a set Z_m contains relevant, redundant, and unnecessary features, i.e., $X_1, X_2, X_3, \ldots X_m$, where m is the total number of elements of the set. The selection algorithm provides a subset of n elements, Z_n which are those n elements that have the most relevant features within Z_m. To select the subset Z_n, a selection criterion J has to be defined.

If J is monotonic, any subset of features should have a value of J that is less than or equal to that of any proper superset or superset. However, excluding a particular feature from a large set may not significantly impact the criterion values (i.e., number of DOF). Therefore, each feature in the m-feature superset (Z_m in Fig. 1) is removed (one at a time), and the value of J is evaluated for each of the resulting subsets at level 1 in Fig. 1. The subset with the maximum value of $J(Z_{m-1})$ at level 1 is selected, and all other subsets are discarded. All subsets of Z_{m-1} at level 2 have a value of J that is less than or equal to that of Z_{m-1}. The subset of Z_{m-1} (at level 2 in Fig. 1) with the maximum value of $J(Z_{m-2})$ is selected, while others are discarded. This process of selecting the subset with the maximum value of J and discarding all others is repeated until the desired number of features is selected. In this study, the number of DOF for a set of features under consideration is the selection

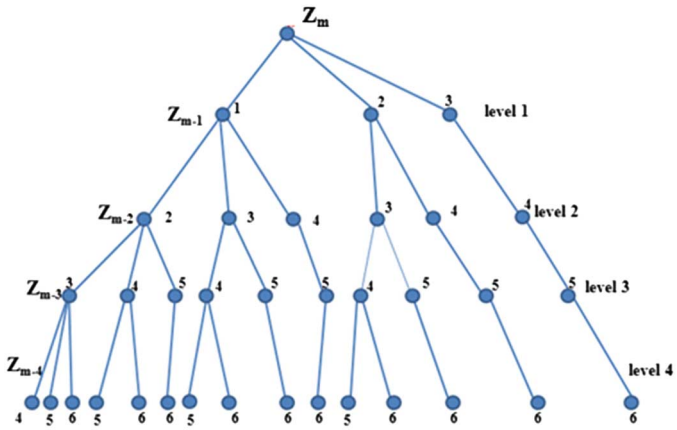

Fig. 1. Solution tree based on a branch and bound feature selection algorithm.

criterion, where features are the WFs corresponding to various frequencies.

The averaging kernel is calculated using (5) [13], and the number of DOF is calculated as the trace of the averaging kernel matrix (6) [13]

$$\overline{\overline{AK}} = \overline{\overline{S}}_a \overline{\overline{WF}}^T \left(\overline{\overline{WF}}\, \overline{\overline{S}}_a \overline{\overline{WF}}^T + \overline{\overline{S}}_\varepsilon \right)^{-1} \overline{\overline{WF}} \tag{5}$$

$$DOF = tr\left(\overline{\overline{AK}}\right) \tag{6}$$

where

$\overline{\overline{S}}_a$ background information covariance matrix, with dimensions depending on the number of layers used for the retrieval and with values calculated based on the statistics of radiosonde profiles.

$\overline{\overline{WF}}$ weighting function matrix.

$\overline{\overline{S}}_\varepsilon$ measurement error covariance matrix. The measurements at each of the frequencies are independent of each other, so the errors associated with the measurements are also independent.

$\overline{\overline{S}}_\varepsilon$ includes the noise due to radiometric observations, representativeness error, and radiative transfer model errors [14]. However, the off-diagonal elements are assumed to be negligible in this study, and the radiometer instrument noise is considered to be 0.5 K. In addition, in the later part of this study for determining the impact of measurement error on DOF and vertical resolution, variable measurement noise has been used and the effects of representativeness error and radiative transfer model error have also been included [14].

In this paper, the feature selection algorithm evaluates a set of WFs corresponding to the frequency range from 10 to 200 GHz to determine the major contributing frequencies for remote sensing of water vapor and temperature profiles. In this study, the value of m is 1900, and the frequency selection process is repeated for values of n equal to 2, 3, 4, 5, 10, 20, 30, 40, and 50.

B. Averaging Kernel and Vertical Resolution

The vertical resolution of a retrieved profile is defined as the spread of its averaging kernel, given by (7). The averaging kernel is a linear combination of WFs for the frequencies used in the study, as shown in (8) [13]

$$sp(z) = 12 \int (z - z')^2 \left[\sum_{i=1}^{m} \overline{\overline{WF}}_i (z')\, G_a(z) \right]^2 dz' \tag{7}$$

$$AK(z, z') = \int \sum_{i=1}^{m} \overline{\overline{WF}}_i (z')\, G_a(z) dz'. \tag{8}$$

The spread of an averaging kernel can be rewritten as

$$sp(z) = G_a(z)^T \overline{\overline{Q}}_a(z) G_a(z) \tag{9}$$

where $G_a(z)$ is the gain function (containing coefficients for a linear combination of WFs), and $\overline{\overline{Q}}_a$ is given by

$$\overline{\overline{Q}}_{aij}(z) = 12 \int (z - z')^2 \overline{\overline{WF}}_i (z')\, \overline{\overline{WF}}_j (z')\, dz' \tag{10}$$

where the $\overline{\overline{Q}}_a$ matrix elements are the correlations between values of the WFs at two different frequencies (i and j) at various altitudes z. $\overline{\overline{WF}}$ is the WF, z is the height above ground level, i and j are the indices of the frequency channels, and z' is the height above ground level of the center of the averaging kernel.

Achieving optimal vertical resolution requires minimizing the spread of the averaging kernel. An ideal averaging kernel would be a Dirac delta function. However, the spread of an averaging kernel is determined based on a finite number of WFs (for different weather conditions) at the corresponding frequencies of measurement. The limited number of WFs makes it virtually impossible to achieve a delta function as an averaging kernel. To address this limitation, the Backus–Gilbert technique improves the vertical resolution by using a gain function, calculated as in (11), to minimize the spread of the averaging kernel. Using (10) and (11) in (9), the spread of the averaging kernel is (12) [13]

$$\bar{g}_a(z) = \frac{\overline{\overline{Q}}_a^{-1}(z)\bar{u}}{\bar{u}^T \overline{\overline{Q}}_a^{-1}(z)\bar{u}} \tag{11}$$

$$sp(z) = \frac{1}{\bar{u}^T \overline{\overline{Q}}_a^{-1} \bar{u}} \tag{12}$$

where the elements of $\bar{u}$ are given by

$$u_i = \int_0^{10\,km} \overline{\overline{WF}}_i\, dz. \tag{13}$$

III. Analysis of Water Vapor and Temperature Measurements From Zenith-Pointing Ground-Based Radiometers

A. Effect of Liquid Water on Temperature and Water Vapor Profile Retrieval

Brightness temperature measurements near weak (22.235 GHz) and strong (183.31 GHz) water vapor absorption lines have significant contributions from cloud liquid water

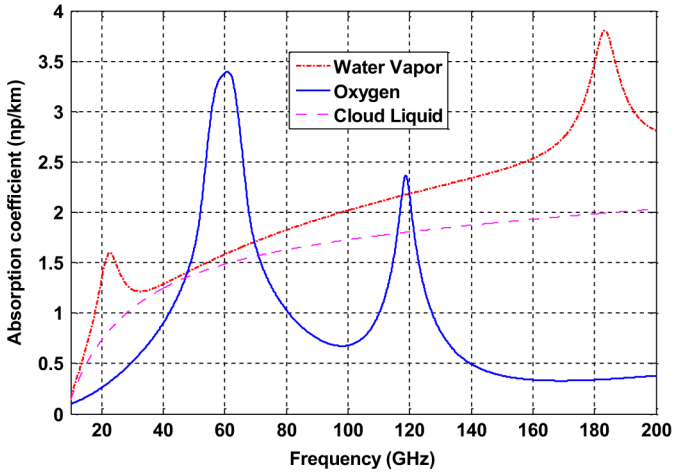

Fig. 2. Microwave and millimeter-wave absorption spectra from 10 to 200 GHz for water vapor density of 15.1 g/m^3, temperature of 297 K and cloud liquid water density of 0.1 g/m^3.

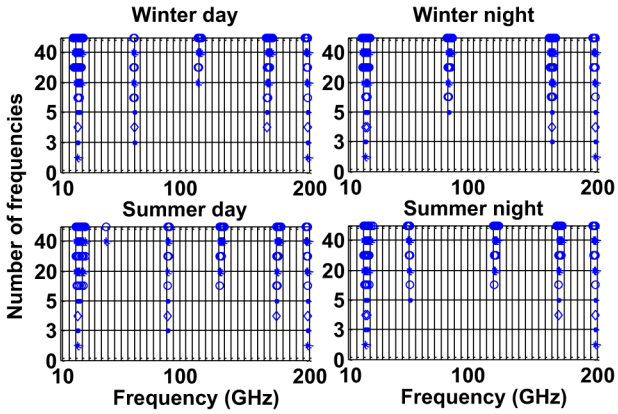

Fig. 3. Main contributing frequencies for water vapor profile retrieval from a ground-based radiometer determined using the feature selection method for the frequency range of 10–200 GHz. The width of the horizontal axis divisions is 5 GHz.

and precipitation, when present, which can be major sources of error in water vapor retrieval. The contributions from clouds and precipitation can be due to scattering and/or absorption at microwave and millimeter-wave frequencies. Fig. 2 shows microwave and millimeter-wave absorption spectra of water vapor, oxygen, and liquid water absorption coefficients for 10–200 GHz.

Typically, scattering occurs in nonprecipitating ice clouds, whereas absorption occurs in liquid clouds. The emission by clouds is also affected by cloud thermodynamic temperature [15]. Cloud liquid is a significant contributor to measured brightness temperature near the weak water vapor absorption line at 22.235 GHz. However, water drops in clouds can be very small compared to the wavelength of the radiation, so the Rayleigh approximation can be used. Based on this approximation, scattering can be neglected in the forward radiative transfer equations, so only absorption models are used [16]. Water vapor profile retrieval with current methods is highly inaccurate during precipitation [17], unless specifically tuned for it [18]. For this reason, in this study, cloudy conditions have not been considered, and all the cases used in this study are for clear sky conditions.

B. Determining Measurement Frequencies for Ground-Based Water Vapor Profiling

A branch and bound feature selection technique is applied to the water vapor WFs calculated using (1) for frequencies in the range from 10 to 200 GHz. As described in Section II, WFs have been calculated using radiosondes launched from the ARM SGP site. These WFs have been calculated for four "typical" weather conditions, i.e., winter day/night and summer day/night based on radiosondes launched during December/January and June/July for winter and summer, respectively, and at noon/midnight for day/night, respectively. The frequencies selected for each value of n are shown in Fig. 3, where n is the number of main contributing frequencies, as defined in Section II-A.

For any of these four combinations of season and time of day, frequencies near the weak water vapor absorption line at 22.235 GHz are selected as the first contributing measurement frequency for water vapor sensing, in agreement with previous work [7]. The first 10 selected frequencies for water vapor retrieval in each case are given in Table I. Similarly, frequencies relatively close to the strong water vapor absorption line at 183.31 GHz are selected as the second contributing frequency, near 200 GHz. When the number of frequencies to be selected is greater than 2, the frequencies selected vary with the season and time of the day. When the number of frequencies selected is 3 and 4, frequencies near 90 and 165 GHz are also selected along with the frequencies near 23 and 183 GHz.

TABLE I
FIRST 10 FREQUENCIES (IN GHZ) SELECTED FOR WATER VAPOR PROFILE RETRIEVAL FROM GROUND-BASED MEASUREMENTS FOR WINTER DAY/NIGHT AND SUMMER DAY/NIGHT CONDITIONS

Winter day	21.3	198.9	65.3	167.7	22.9	168.1	21.7	22.5	23.3	64.9
Winter night	21.3	198.9	165.3	22.9	85.7	164.9	165.7	85.3	22.5	23.3
Summer day	21.3	198.9	90.5	174.9	22.9	175.3	131.3	20.5	24.1	25.7
Summer night	21.3	198.9	22.9	170.1	55.7	170.5	120.5	20.5	22.5	24.1

The selected frequencies were analyzed to determine the number of independent pieces of information by calculating their number of DOF using (5) and (6). The parameters required for the averaging kernel in (5), i.e., background covariance matrix $\overline{\overline{S}}_a$ and WF matrix $\overline{\overline{WF}}$, are calculated using a background data set of radiosonde profiles measured at the ARM SGP site [9]. The background data set is a collection of water vapor and temperature profiles for the appropriate season and time of the day, i.e., winter day/night or summer day/night for this study. Similarly, WFs are calculated using mean water vapor and temperature profiles from the same data set. The number of DOF is calculated for each set of selected frequencies based on the value of n. This process is followed for a number of background data sets, and the resulting mean and standard deviation for each value of n are shown in Fig. 4. It can be seen that the number of DOF is slightly lower during winter than during summer, for both day and night. This is because

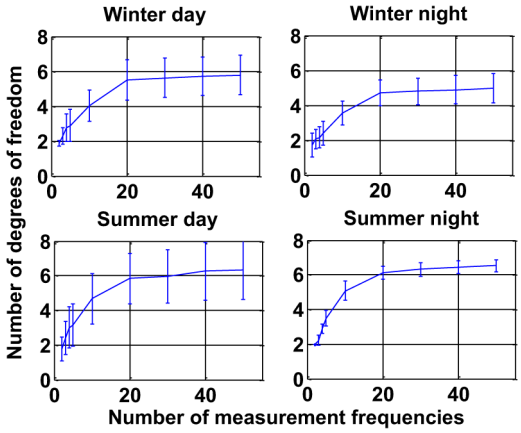

Fig. 4. Number of DOF for water vapor profile retrieval from ground-based radiometer measurements under four different clear-sky weather conditions, i.e., winter day/night and summer day/night, for the frequency range of 10–200 GHz.

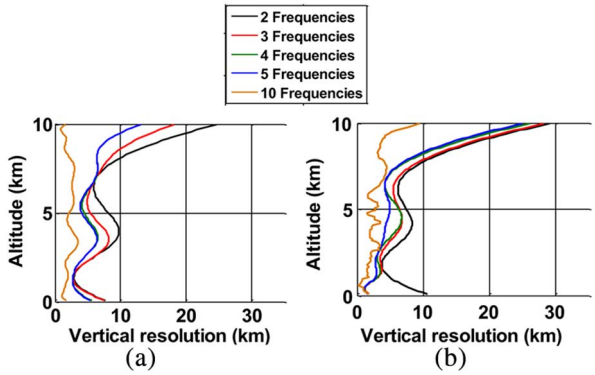

Fig. 5. Vertical resolution for water vapor profile retrieval from a ground-based radiometer as a function of altitude for (a) winter and (b) summer daytime.

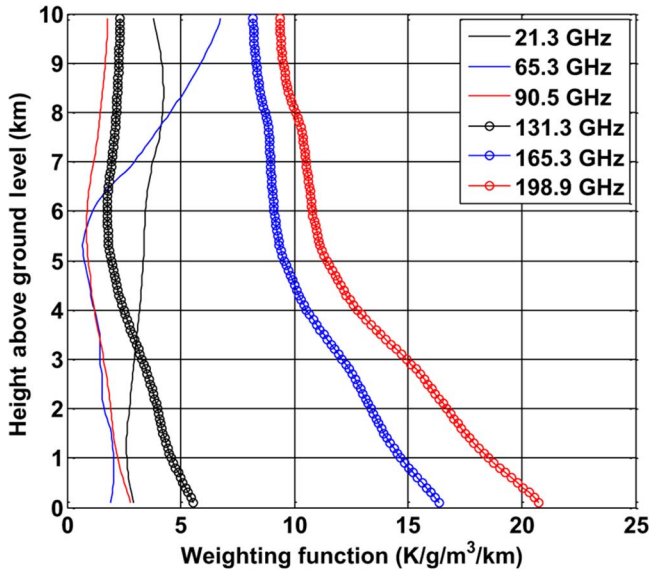

Fig. 6. WFs for the frequencies selected for water vapor profile retrieval from ground-based radiometer measurements in the range from 10 to 200 GHz.

water vapor profiles are more variable during summer than during winter. When the number of frequencies selected is in the range of 2–5, the mean number of DOF increases linearly with the number of selected frequencies. When the number of frequencies selected is in the range of 5–20, the number of DOF continues to increase, but at a much slower rate. For the range of 20–50 frequencies, the number of DOF saturates. The range of maximum number of DOF (for a mean profile) is 5–6.2 for any atmospheric condition. Hence, increasing the number of selected frequencies of measurement above a certain value does not significantly increase the number of independent pieces of information. For example, the number of DOF increases by only one or two as the number of measurement frequencies is increased from 10 to 40.

It is also important to determine the vertical resolution of the retrieval using the selected frequencies. In this study, vertical resolution is defined as spread of the averaging kernel based on the Backus–Gilbert technique, as described in Section II-B. Vertical resolution is computed as the spread of the averaging kernel for the first two frequencies selected for winter and summer daytime using (12) for a height range of 0–10 km above ground level, as shown by the black curves in Fig. 5(a) for winter and (b) for summer. Similarly, the vertical resolution is calculated for the first three selected frequencies, as shown by the red curves in Fig. 5. This process is continued for 4, 5, and 10 selected frequencies.

There is a general trend of degradation in vertical resolution as the altitude increases. However, the spread decreases (and vertical resolution improves) as the number of selected frequencies increases. The vertical resolution for 10 measurements is approximately 0.5–1.5 km from 0 to 2 km above ground level for both winter and summer. However, from 2 to 9 km above ground level the vertical resolution for 10 measurements is approximately 1.5–3 km.

The WFs corresponding to the frequencies contributing the greatest number of independent pieces of information as well as improving the vertical resolution of water vapor profile retrieval are shown in Fig. 6.

WFs corresponding to 131.3, 165.3, and 198.9 GHz show that these measurement frequencies are sensitive to water vapor in the lower parts of the troposphere and hence are complementary to 21.3 GHz for estimation of water vapor profiles. Frequencies closer to the strong water vapor absorption line are more sensitive to changes in water vapor close to the ground. The WF at 198.9 GHz is highly sensitive to small changes in water vapor, as noted by Cimini *et al.* [19] and Racette *et al.* [20]. This and similar frequencies are useful to retrieve the water vapor profile in very dry climates, such as the polar regions [19]. Measurements close to 90.5 GHz in the window region from approximately 85–110 GHz have been used to estimate the total precipitable water, as described by Payne *et al.* [21].

C. Determining Measurement Frequencies for Ground-Based Temperature Profiling

Temperature profiles have been retrieved from satellite-based radiometric measurements in the range from 50 to 70 GHz [22],

TABLE II
FIRST 10 FREQUENCIES (IN GHZ) SELECTED FOR TEMPERATURE PROFILE RETRIEVAL FROM GROUND-BASED MEASUREMENTS FOR WINTER DAY/NIGHT AND SUMMER DAY/NIGHT CONDITIONS

Winter day	60.1	118.1	55.7	119.3	67.3	119.7	63.3	116.9	67.7	116.1
Winter night	60.5	118.1	63.3	62.5	118.9	116.9	64.9	55.3	65.7	66.1
Summer day	60.1	117.7	62.5	116.5	64.5	118.1	118.5	119.3	119.7	116.1
Summer night	60.1	118.1	62.5	116.5	119.3	117.7	119.7	61.7	64.5	116.1

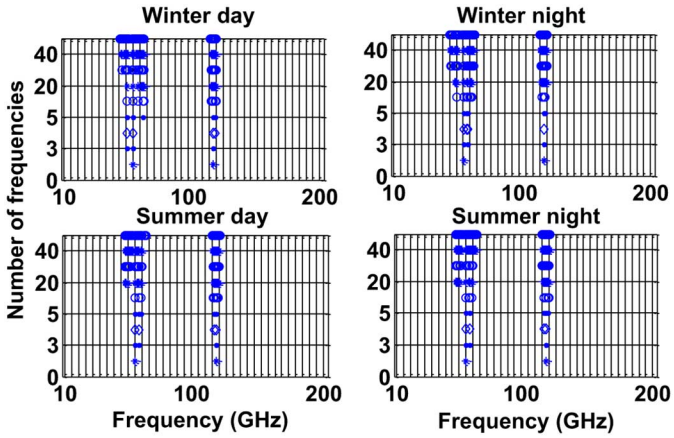

Fig. 7. Main contributing frequencies for temperature profile retrieval from a ground-based radiometer determined using the feature selection method for the frequency range of 10–200 GHz. The width of the horizontal axis divisions is 5 GHz.

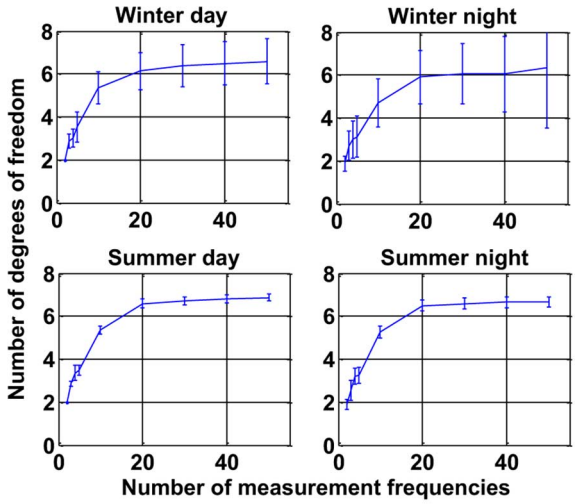

Fig. 8. Number of DOF for temperature profile retrieval from a ground-based radiometer under four different clear-sky weather conditions, i.e., winter day/night and summer day/night, for the frequency range of 10–200 GHz.

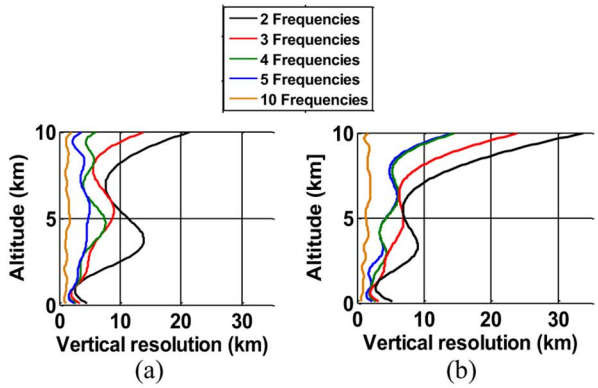

Fig. 9. Vertical resolution for temperature profile retrieval from a ground-based radiometer as a function of altitude for (a) winter and (b) summer daytime.

i.e., near the oxygen absorption complex centered at 60 GHz. Measurements at frequencies further away from the 60-GHz oxygen complex provide information about the temperature at lower altitudes, based on the temperature WFs. Frequencies near the higher frequency millimeter-wave oxygen absorption line at 118.75 GHz have not been used extensively for temperature profiling. Also, the window region frequencies between these absorption lines have not been analyzed in detail for temperature retrieval. To include them in this study, the entire frequency range of 10–200 GHz has been analyzed to determine sets of frequencies that provide the maximum amount of information on tropospheric temperature profiles.

Similar to the retrieval of water vapor profiles, retrieval of temperature profiles also requires the maximum number of independent pieces of information (or minimum redundancy) to improve accuracy and sensitivity to changes in temperature as a function of altitude. The major contributing frequencies were selected by applying a feature selection algorithm (similar to that used for water vapor selection in Section III-B) to the temperature WFs corresponding to frequencies in the range from 10 to 200 GHz.

The first 10 selected frequencies are listed in Table II and shown in Fig. 7.

Frequencies close to 60 GHz have greater information content and provide more independent measurements than those close to the oxygen absorption line at 118.75 GHz. For all weather conditions considered in this study, the frequency ranges of 55–65 GHz and 116–120 GHz are selected, which are close to the 60-GHz oxygen complex and the 118.75-GHz oxygen absorption line, respectively.

The selected frequencies were analyzed to determine the number of independent pieces of information by calculating their number of DOF, as shown in Fig. 8.

The number of DOF increases approximately linearly with the increase in the number of frequencies selected up to 10 and then increases more slowly up to 20. The number of DOF starts to saturate near or above 30 selected frequencies. The maximum number of mean DOF is approximately 6–7 for temperature profile retrieval from zenith-pointing ground-based radiometers, under nearly all clear-sky weather conditions considered in this study.

However, the mean maximum number of DOF is slightly higher for summer (6.7) than for winter (6.4), which is a similar relationship to that in Section III-B (Fig. 4) for water vapor measurements. This is due to the greater variability of temperature profiles in summer than in winter. After examining the number of DOF, the vertical resolution was analyzed for the

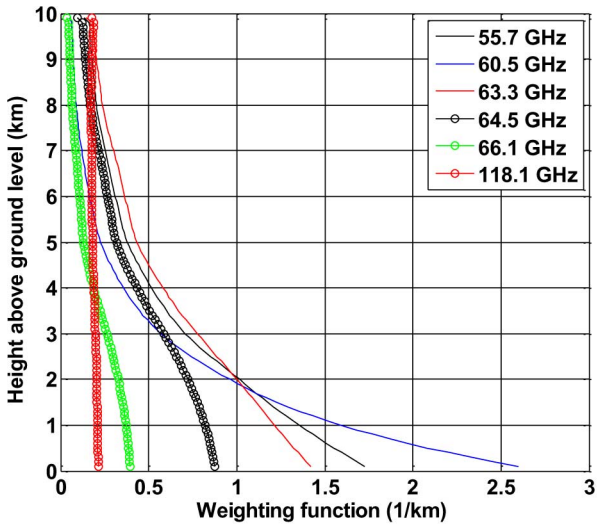

Fig. 10. Temperature WFs for frequencies selected for temperature profile retrieval from ground-based radiometer measurements in 10–200 GHz range.

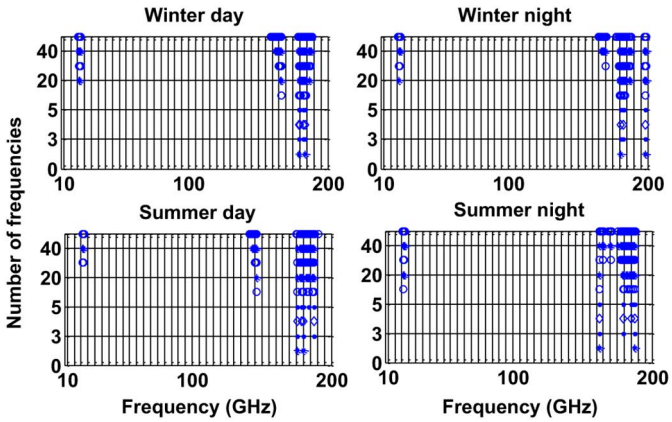

Fig. 11. Main contributing frequencies for water vapor retrieval from airborne measurements selected using the feature selection method for the frequency range of 10–200 GHz. The width of the horizontal axis divisions is 5 GHz. The bandwidth is assumed to be 100 MHz.

TABLE III
FIRST 10 FREQUENCIES (IN GHZ) SELECTED FOR WATER VAPOR PROFILE RETRIEVAL FROM AIRBORNE MEASUREMENTS FOR WINTER DAY/NIGHT AND SUMMER DAY/NIGHT CONDITIONS

Winter day	179.3	184.1	182.5	180.1	183.3	183.7	184.7	180.9	180.5	166.9
Winter night	190.5	198.9	191.3	174.9	182.9	175.3	180.5	181.3	184.1	185.7
Summer day	175.7	179.7	187.3	178.9	183.7	186.5	186.9	187.3	182.5	146.5
Summer night	162.1	187.3	179.3	184.9	186.5	182.5	179.7	186.1	183.7	21.3

selected frequencies for temperature profiling, similar to what was done for water vapor profiling. The spread of the averaging kernel is determined for first 2, 3, 4, 5, and 10 frequencies selected for temperature profiling during daytime, as shown by the black, red, green, blue, and gold curves, respectively, in Fig. 9(a) for winter and (b) for summer. There is a general degradation in vertical resolution as the altitude increases. However, the vertical resolution decreases as the number of frequencies selected increases. The vertical resolution for 10 measurements is approximately 0.2–0.5 km from the ground to 4 km above ground level.

Fig. 10 shows the WFs for the frequencies selected for temperature profile retrieval. Most of the WFs are most sensitive to temperature changes in the lowest 2 km of the troposphere.

The 55.7, 60.5, and 63.3 GHz frequencies are most sensitive to changes in temperature from the ground to 2 km above ground level, whereas the frequencies 64.5 and 66.1 GHz (further from the 60-GHz oxygen complex) are generally more sensitive to changes in temperature from the ground to 4 km above ground level. None of the WFs studied in this section have much sensitivity to changes in temperature above about 7 km above ground level.

IV. ANALYSIS OF WATER VAPOR AND TEMPERATURE MEASUREMENTS FROM NADIR-POINTING AIRBORNE RADIOMETERS

This section focuses on determining the measurement frequencies in the range from 10 to 200 GHz to provide the maximum number of independent measurements for water vapor and temperature profile retrievals for a nadir-pointing airborne microwave radiometer. For the study in Sections IV-C1 and IV-C2, the background temperature is assumed to be 290 K and the emissivity of the sea surface to be 0.5. However, in Section IV-C2, an analysis has been performed to determine the variability in the number of DOF due to variations in sea and land surface emissivity. The altitude of the aircraft is assumed to be at least 10 km above ground level.

A. Determining Measurement Frequencies for Airborne Water Vapor Profiling

Again, the branch and bound feature selection algorithm was applied to water vapor WFs in the range from 10 to 200 GHz to determine the major contributing frequencies for retrieval of water vapor profiles. The first 10 selected major contributing frequencies for a nadir-pointing airborne radiometer are shown in Fig. 11 and listed in Table III.

The plots show that there are major contributions from frequencies from 180 to 200 GHz for all clear-sky weather conditions studied, but there are also some significant contributors in the window region in the range of 130–165 GHz. Measurements in the latter frequency range can be used for accurate retrieval of profiles of water vapor in the upper troposphere (5–10 km) where the water vapor density is less than $0.5\,\mathrm{g/m^3}$. This is because frequencies close to the strong water vapor absorption line are highly attenuated, even when a small amount of water vapor is present.

However, the atmosphere is more transparent near the weak water vapor absorption line (in the range of 20–23 GHz), so 21.3 GHz can be used for retrieval of water vapor profiles in the lowest 10 km of the troposphere. The number of DOF calculated for each value of n (from 2 to 50) corresponding to

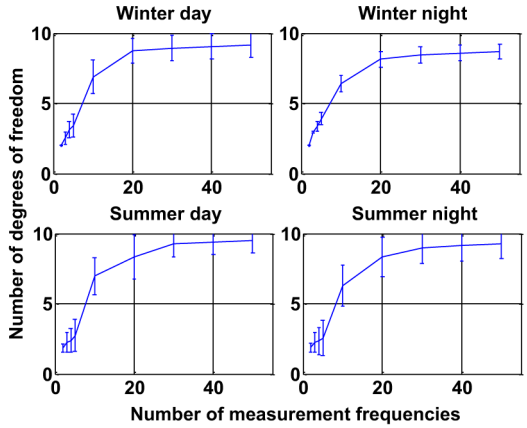

Fig. 12. Number of DOF for water vapor profile retrieval from airborne measurements under four different clear-sky weather conditions, i.e., winter day/night and summer day/night, for the frequency range of 10–200 GHz.

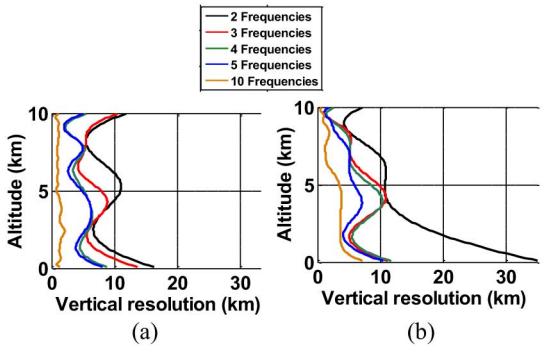

Fig. 13. Vertical resolution for water vapor profile retrieval from airborne measurements as a function of altitude for (a) winter and (b) summer daytime.

all weather conditions studied is shown in Fig. 12. The maximum number of mean DOF for all weather conditions studied is approximately 8–9, lowest for winter night and highest for summer day. The maximum number of mean DOF is greater than that for zenith-pointing ground-based radiometers.

The vertical resolution is computed for frequencies selected for water vapor profile retrieval using a nadir-pointing airborne radiometer. The spread of the averaging kernel determined for first 2, 3, 4, 5, and 10 frequencies selected for daytime is shown by the black, red, green, blue, and orange curves, respectively, in Fig. 13(a) for winter and (b) for summer.

The vertical resolution in this case is better at 10 km above ground level than at ground level due to the difference in the radiative transfer integral, resulting in nadir-pointing airborne and spaceborne radiometers providing more information in the upper troposphere.

The vertical resolution is best for 10 measurements and is approximately 0.2–0.5 km from 6 to 10 km above ground level for winter, and it is 0.2–1 km for similar altitudes in summer. The vertical resolution is degraded closer to the ground.

WFs corresponding to the major contributing frequencies are shown in Fig. 14. Those corresponding to frequencies close to the strong water vapor absorption line at 183.31 GHz as well as the window channels peak at various altitudes, are most

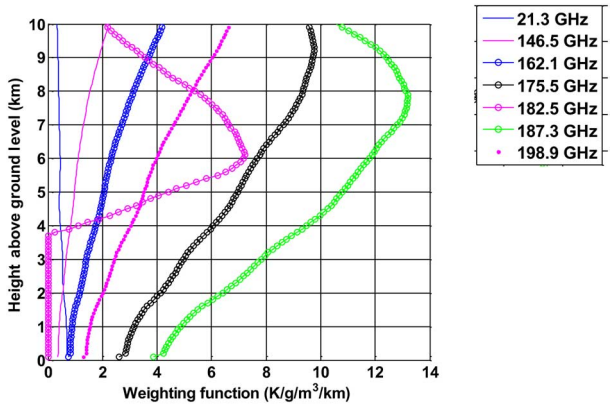

Fig. 14. Water vapor weighting functions for frequencies selected for water vapor profile retrieval from nadir-pointing airborne measurements in the 10–200 GHz range.

TABLE IV
FIRST 10 FREQUENCIES (IN GHZ) SELECTED FOR TEMPERATURE PROFILE RETRIEVAL FROM AIRBORNE MEASUREMENTS FOR WINTER DAY/NIGHT AND SUMMER DAY/NIGHT CONDITIONS

Winter day	60.1	117.7	54.9	56.9	56.5	118.1	64.5	59.7	55.3	52.9
Winter night	60.1	117.7	55.3	56.9	56.5	118.1	64.5	57.7	59.7	54.9
Summer day	60.1	117.7	55.7	55.3	118.1	60.5	59.7	56.9	56.5	54.9
Summer night	60.1	117.7	55.3	56.5	118.1	60.5	59.7	56.9	55.7	54.9

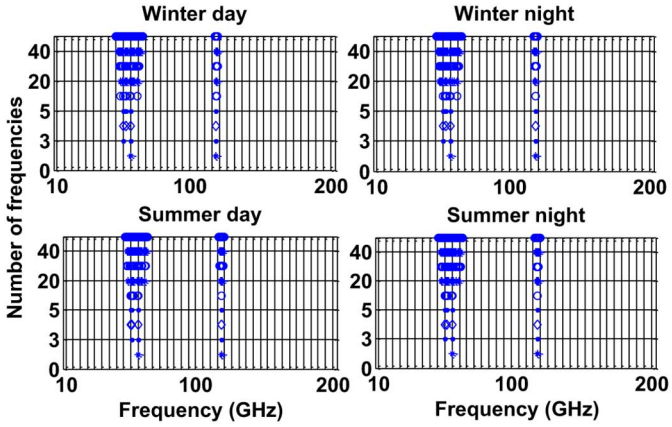

Fig. 15. Main contributing frequencies for temperature profiling from airborne measurements selected using the feature selection method for the frequency range 10–200 GHz. The width of the horizontal axis divisions is 5 GHz. The bandwidth is assumed to be 100 MHz.

sensitive to changes above 4 km altitude and can be used for retrieval of water vapor profiles in the upper troposphere.

B. Determining Measurement Frequencies for Airborne Temperature Profiling

Analysis of the temperature WFs in the range of 10–200 GHz results in the first 10 frequencies selected for a nadir-pointing airborne radiometer shown in Table IV and Fig. 15. They show that frequencies close to 60 and 118.75 GHz temperature

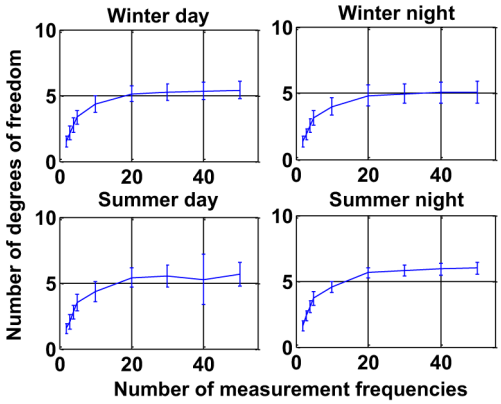

Fig. 16. Number of DOF for temperature profile retrieval from airborne measurements under four different clear-sky weather conditions, i.e., winter day/night and summer day/night, for the frequency range of 10–200 GHz.

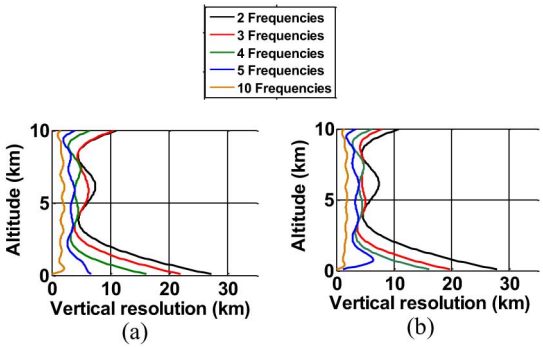

Fig. 17. Vertical resolution for temperature profile retrieval from airborne measurements as a function of altitude for (a) winter and (b) summer daytime.

absorption lines provide the greatest amount of information for temperature profile retrieval from nadir-pointing airborne radiometers.

The number of independent pieces of information from the selected frequency set can be determined by calculating the number of DOF for each weather condition studied, as shown in Fig. 16. The maximum number of mean DOF for all weather conditions studied is approximately 5–6 for temperature profile retrieval from an airborne radiometer. The number of DOF increases as the number of measurements is increased from 2 to 20, but there is no significant increase in number of DOF for more than 20 measurements.

The spread of the averaging kernel is computed for temperature profile retrieval from nadir-pointing airborne radiometer measurements. The vertical resolution is determined for first 2, 3, 4, 5, and 10 frequencies selected shown by the black, red, green, blue, and gold curves, respectively, in Fig. 17. Similar to water vapor retrieval from nadir-pointing airborne measurements, the vertical resolution in this case is better at 10 km above ground level than it is at ground level. The vertical resolution is best for 10 measurements and is approximately 0.2–0.5 km in winter from 6 to 10 km above ground level and 0.2–1 km for similar altitudes in summer.

WFs for the major contributing frequencies are shown in Fig. 18. The WFs corresponding to 55.3, 56.9, and 60.1 GHz

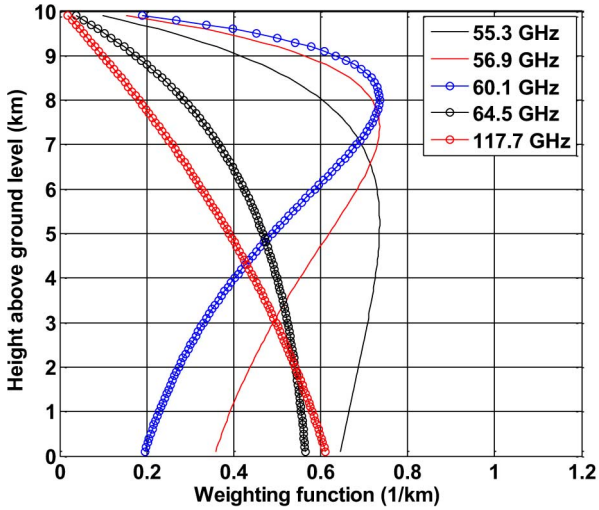

Fig. 18. Temperature WFs for nadir-pointing airborne measurement frequencies in the range of 10–200 GHz.

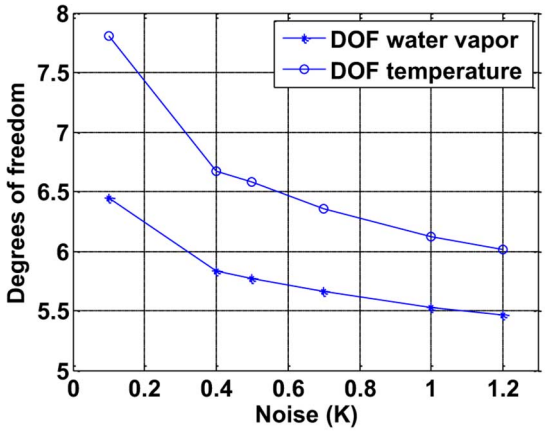

Fig. 19. Variation in the number of DOF for a range of instrument noise values for a zenith-pointing ground-based microwave radiometer.

peak at various altitudes well above ground level and hence can be used to retrieve temperature profiles. The WFs at 64.5 and 117.7 GHz are more sensitive to temperature in the lowest 2 km of the troposphere and therefore are complementary to the frequencies closer to the 60-GHz oxygen complex.

C. Effect of Variation in Measurement Noise and Uncertainty on the Number of Independent Measurements and Vertical Resolution

1) Effect of Variation in Instrument Noise on the Number of DOF: All of the previous results have been calculated assuming a radiometric resolution of 0.5 K and a diagonal matrix $\overline{\overline{S}}_{\varepsilon}$. However, in this section, an analysis has been performed to determine the variation in the number of DOF for 50 measurement frequencies selected using the branch and bound selection algorithm described in Section III for a zenith-pointing ground-based radiometer when the instrument noise is varied from 0.1 to 1.2 K. The results are shown in Fig. 19. The number of DOF decreases from 7.8 to 6 for temperature measurement

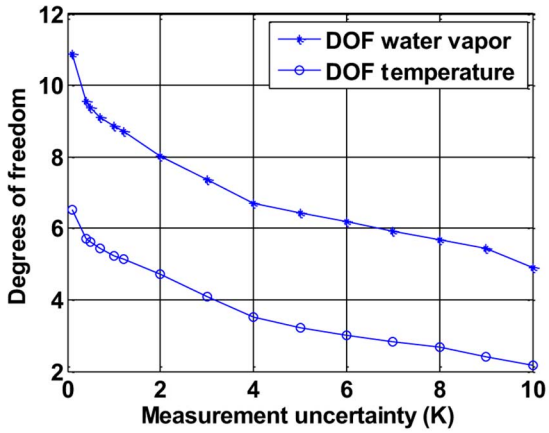

Fig. 20. Variation in the number of DOF for a range of measurement uncertainties for a nadir-pointing airborne radiometer at 10 km above ground level.

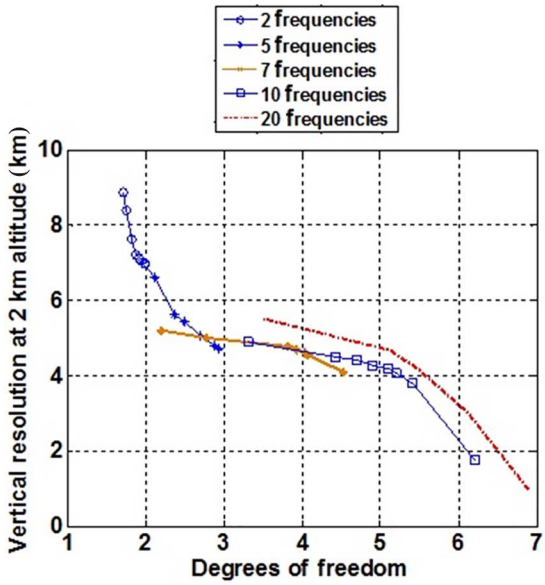

Fig. 21. Variation in the number of DOF and vertical resolution with noise for a zenith-pointing ground-based radiometer.

frequencies, whereas the number of DOF decreases from 6.45 to 5.5 for water vapor measurement frequencies as the instrument noise is increased from 0.1 to 1.2 K. Therefore, an increase in instrument noise has a negative effect on the number of DOF, as expected.

2) Effect of Variation in Measurement Uncertainty on the Number of DOF for an Airborne Radiometer: Airborne microwave radiometer measurements are affected by variations in atmospheric conditions as well as by the emissivity of land and sea surfaces. Measurements performed by an airborne microwave radiometer can be represented by

$$T_{B_{Measured}} = T_{B_{Ideal}} + \varepsilon_{T_B} \tag{14}$$

where $T_{B_{Measured}}$ is the measurement, $T_{B_{Ideal}}$ is the measurement due to atmospheric parameters, and ε_{T_B} is the uncertainty associated with the measurement, representativeness error and radiative transfer model errors. The uncertainty in the measurement is due to instrument noise, and the uncertainty associated with the land and sea surface emissivity is shown below

$$\varepsilon_{T_B} = \Delta T_B + T_{B_{Surface\_uncertainty}} \tag{15a}$$

$$\varepsilon_{T_B} = \Delta T_B + (1-\epsilon)\, T_B^{\downarrow} + \epsilon T_{ph} + \varepsilon_r \tag{15b}$$

where ΔT_B is the uncertainty due to measurement noise, ϵ is the land emissivity, $T_B{}^{\downarrow}$ is the downwelling brightness temperature measured at ground level, T_{ph} is the surface temperature, and ε_r represents the uncertainty due to representativeness error and radiative transfer model errors.

Emissivity models of land and sea surfaces can be used to reduce the emissivity uncertainty. However, some residual error will persist. The effect of uncertainty on the number of DOF of measurements is analyzed and is shown in Fig. 20. The figure shows the variation in the number of DOF for 50 measurement frequencies when the measurement uncertainty is increased from 0.1 to 10 K. The number of DOF decreases from 10.9 to 4.9 for water vapor measurement frequencies as the uncertainty is increased from 0.1 to 10 K. Similarly, the number of DOF for temperature measurement frequencies decreases from 6.7 to 2.2 as the uncertainty is increased from 0.1 to 10 K. Lower values of uncertainty estimate the effect of variation in sea surface emissivity. However, high values of uncertainty estimate the effect of variation in land surface emissivity.

3) Effect of Variation in Measurement Uncertainty on the Number of DOF and Vertical Resolution: The vertical resolution of the measurements has been optimized in Sections III and IV using the Backus–Gilbert method without taking the measurement error into account. Measurement error affects the vertical resolution as well as the number of DOF. Therefore, a study has been performed in which the measurement noise is varied from 0.1 to 1.2 K and its impact on the number of DOF and vertical resolution at 2 km above ground level for a ground-based radiometer and 8 km above ground level for an airborne radiometer is analyzed for $n = 2,\ 5,\ 7,\ 10,$ and 20 measurements.

To include the impact of noise, the gain function is changed according to (16) and substituted into (9)

$$\overline{g_a}(z) = \frac{\left(\overline{\overline{Q}}_a(z) + \overline{\overline{S}}_\varepsilon\right)^{-1}\bar{u}}{\bar{u}^T\left(\overline{\overline{Q}}_a(z) + \overline{\overline{S}}_\varepsilon\right)^{-1}\bar{u}}. \tag{16}$$

The results of the analysis are shown in Figs. 21 and 22, which relate the number of DOF to vertical resolution for ground-based and airborne radiometers, respectively. The leftmost end of each curve in Fig. 21 shows the case when the noise is maximum, and the rightmost end of the curve shows the case when the noise is minimum. As the noise of the system is decreased, the number of DOF increases and the vertical resolution at 2 km above ground level improves. For two measurement frequencies for a ground-based radiometer, as the noise is reduced from 1.2 to 0.1 K, the number of DOF increases from 1.7 to 2 while the corresponding vertical resolution improves from 8.8 to 7 km. Similarly, for 7 measurement frequencies, the number of DOF increases from 2.5 to 4.5 and

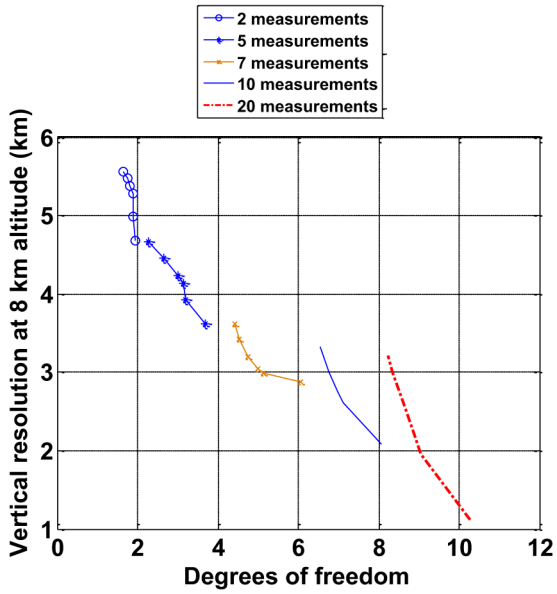

Fig. 22. Variation in the number of DOF and vertical resolution with noise for a nadir-pointing airborne radiometer.

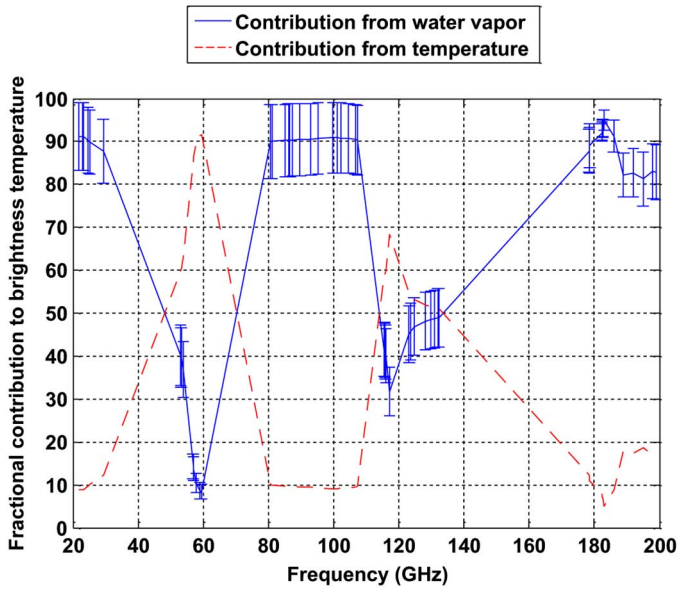

Fig. 23. Fractional contributions of water vapor and temperature to total brightness temperature measurements.

the vertical resolution improves from 5.4 to 4 km. For 10 measurements, the vertical resolution improves from 4.8 to 1.7 km and the number of DOF increases from 2.8 to 6.3. For 20 measurements, the number of DOF increases from 3.5 to 6.9 and the vertical resolution improves from 5.6 to 1 km.

Fig. 22 shows that for two measurements of an airborne radiometer, as the noise is reduced from 1.2 to 0.1 K, the number of DOF increases from 1.7 to 2, whereas the corresponding vertical resolution improves from 5.6 to 4.6 km for 8 km above ground level. Similarly, for five measurement frequencies, the number of DOF increases from 2.2 to 3.7 and vertical resolution improves from 4.6 to 3.5 km. For 10 measurements, the vertical resolution improves from 3.3 to 2.1 km and the number of DOF increases from 6.5 to 8.0. For 20 measurements, the number of DOF increases from 8.5 to 10.9 and the vertical resolution improves from 3.2 to 1.2 km. These plots show that for assessing vertical resolution the important parameter is the number of DOF. Fewer frequency channels with smaller uncertainty have similar performance to a larger number of frequency channels with greater uncertainty.

V. Orthogonalizing Water Vapor and Temperature Measurements

The feature selection method has been used to determine the frequencies that have the highest number of DOF in the frequency range of 10–200 GHz. However, it is important to note that there are a number of frequencies in that range at which the measured brightness temperature has contributions from both water vapor and temperature. This is because the absorption lines for water vapor and temperature are sometimes similarly close to those frequencies, particularly in the window regions. Therefore, it becomes important to determine the particular frequency channels for measuring water vapor or temperature, i.e., the frequencies for which water vapor and temperature contributions are orthogonal, to identify those with contributions to brightness temperature from water vapor that are significantly larger than those from temperature, and vice versa. To accomplish this, the percentage contribution to the brightness temperature due to water vapor absorption is computed using (17).

This relationship is used to compute the relative contribution of water vapor to the total brightness temperature

$$\text{Percentage water vapor contribution} = \frac{T_{Bwv}}{T_{Btotal}} \times 100 = \frac{\rho . W_{wv}}{T . W_T + \rho . W_{wv}} \times 100 \quad (17)$$

for each frequency. It has already been observed that water vapor provides a strong contribution to brightness temperature measurements in the frequency ranges of 20–23 GHz and 165–200 GHz.

These frequency ranges can be used to determine the major contributing channels. To calculate the contribution, 10 radiosonde measurements were performed at the ARM site. The contribution from water vapor is shown in blue in Fig. 23, and the contribution from temperature is shown in red.

Frequencies in the ranges of 20–23, 80–108, and 175–184 GHz have water vapor contributions of more than 90%. Temperature contributes only 10% or less to the total brightness temperature in those frequency ranges. For the frequency ranges of 50–70 and 115–130 GHz, the contribution due to temperature is stronger than that due to water vapor. Frequencies in the ranges of 57–60 and 115–121 GHz have temperature contributions of more than 90% and 60%, respectively. The results presented in Fig. 23 are for a zenith-pointing ground-based radiometer. Similar results were also found for a nadir-pointing airborne radiometer.

VI. Summary and Discussion

Feature selection methods have shown that the frequency ranges of 20–23, 85–90, and 165–200 GHz provide the maximum number of independent pieces of information for water vapor profile retrieval from zenith-pointing ground-based microwave radiometer measurements. The same frequency ranges are useful for water vapor profile retrieval from nadir-pointing airborne radiometers. On the other hand, for temperature profiling from ground-based measurements, the frequency ranges of 55–65 and 116–120 GHz provide the maximum number of independent pieces of information. For temperature profile retrieval from nadir-pointing airborne measurements, nearly the same frequency ranges are needed, but the millimeter-wave frequency range is more narrowly focused near 118.75 GHz.

To determine the number of independent pieces of information and consequently the number of frequencies useful for retrieval of water vapor, the number of DOF has been determined for the selected frequencies in each case. From this analysis, it is found that a limited number of frequency measurements can be used to achieve fine vertical resolution and good accuracy of retrieved water vapor profiles. The maximum number of independent pieces of information is 5–6 for water vapor profiling and 6–7 for temperature profiling from zenith-pointing ground-based radiometer measurements. For nadir-pointing airborne radiometer measurements, the maximum number of independent pieces of information is 8–9 for water vapor profiling and 5–6 for temperature profiling. If additional measurement frequencies are chosen, they will provide redundant information since the information provided is linearly dependent on that already measured at other frequencies. Noise analysis has shown that increasing measurement uncertainty and instrument noise reduces the number of DOF. Similarly, increasing measurement uncertainty degrades the vertical resolution. It was also found that vertical resolution is inversely related to the number of DOF.

References

[1] T. M. Scheve and C. T. Swift, "Profiling atmospheric water vapor with a K-band spectral radiometer," *IEEE Trans. Geosci. Remote Sens.*, vol. 37, no. 3, pp. 1719–1729, May 1999.

[2] E. R. Westwater, S. Crewell, and C. Matzler, "Surface-based microwave and millimeter wave radiometric remote sensing of the troposphere: A tutorial," *IEEE Geosci. Remote Sens. Newslett.*, no. 134, pp. 16–33, Mar. 2005.

[3] N. C. Grody, "Remote sensing of the atmosphere from satellites using microwave radiometry," in *Atmospheric Remote Sensing by Microwave Radiometry*. New York, NY, USA: Wiley-Interscience, 1993, pp. 259–314.

[4] F. S. Solheim *et al.*, "Radiometric profiling of temperature, water vapor, and cloud liquid water using various inversion methods," *Radio Sci.*, vol. 33, pp. 393–404, 1998.

[5] E. R. Westwater, "Ground-based microwave remote sensing of meteorological variables," in *Atmospheric Remote Sensing by Microwave Radiometry*. New York, NY, USA: Wiley-Interscience, 1993, pp. 145–214.

[6] M. A. Janssen, "An introduction to the passive microwave remote sensing of atmospheres," in *Atmospheric Remote Sensing by Microwave Radiometry*. New York, NY, USA: Wiley-Interscience, 1993, pp. 1–35.

[7] A. J. Gasiewski, "Channel ranking in passive microwave wet-path delay measurements," in *Proc. IEEE Geosci. Remote Sens. Symp.*, 1993, pp. 1765–1767.

[8] M. Klein and A. J. Gasiewski, "The sensitivity of millimeter and submillimeter frequencies to atmospheric temperature and water vapor variations," in *Proc. IEEE Geosci. Remote Sens. Symp.*, 1998, pp. 568–571.

[9] M. P. Cadeddu, J. C. Liljegren, and D. D. Turner, "The Atmospheric Radiation Measurement (ARM) program network of microwave radiometers: instrumentation, data and retrievals," *Atmos. Meas. Techn.*, vol. 6, pp. 2359–2372, 2013.

[10] I. Guyon and A. Elisseeff, "An introduction to variable and feature selection," *J.. Mach. Learn. Res.*, vol. 3, pp. 1157–1182, Mar. 2003.

[11] O. Ludwig and U. Nunes, "Novel maximum-margin training algorithms for supervised neural networks," *IEEE Trans. Neural Netw.*, vol. 21, no. 6, pp. 972–984, Jun. 2010.

[12] P. M. Narendra and K. Fukunaga, "A branch and bound algorithm for feature subset selection," *IEEE Trans. Comput.*, vol. C-26, no. 9, pp. 917–921, Sep. 1977.

[13] C. D. Rodgers, *Inverse Methods for Atmospheric Sounding: Theory and Practice*. Singapore: World Scientific, 2000.

[14] T. J. Hewison, *Profiling Temperature and Humidity by Ground-based Microwave Radiometers*. Reading, U.K.: Univ. Reading, 2006.

[15] P. C. Pandey, E. G. Njoku, and J. W. Waters, "Inference of cloud temperature and thickness by microwave radiometry from space," *J. Clim. Appl. Meteorol.*, vol. 22, pp. 1894–1898, Jul. 1983.

[16] D. D. Turner *et al.*, "Retrieving liquid water path and precipitable water vapor from the Atmospheric Radiation Measurement (ARM) microwave radiometers," *IEEE Trans. Geosci. Remote Sens.*, vol. 45, no. 11, pp. 3680–3690, Nov. 2007.

[17] J. A. Weinman, "The effect of cirrus clouds on 118-GHz brightness temperatures," *J. Geophys. Res.*, vol. 93, no. D9, pp. 11059–11062, Sep. 1988.

[18] C. Kummerow *et al.*, "The evolution of the Goddard profiling algorithm (GPROF) for rainfall estimation from passive microwave sensors," *J. Appl. Meteorol.*, vol. 40, pp. 1801–1820, Jun. 2001.

[19] D. Cimini, E. R. Westwater, and A. J. Gasiewski, "Temperature and humidity profiling in the Arctic using millimeter-wave radiometry and 1DVAR," *IEEE Trans. Geosci. Remote Sens.*, vol. 48, no. 3, pp. 1381–1388, Mar. 2009.

[20] P. E. Racette *et al.*, "Measurement of low amounts of precipitable water vapor using ground-based millimeterwave radiometry," *J. Atmos. Ocean. Technol.*, vol. 22, pp. 317–337, Apr. 2005.

[21] V. H. Payne, E. J. Mlawer, K. E. Cady-Pereira, and J. Moncet, "Water vapor continuum absorption in the microwave," *IEEE Trans. Geosci. Remote Sens.*, vol. 49, no. 6, pp. 2194–1388, Jun. 2011.

[22] T. J. Hewison, "1D-VAR retrieval of temperature and humidity profiles from a ground-based microwave radiometer," *IEEE Trans. Geosci. Remote Sens.*, vol. 45, no. 7, pp. 2163–2168, Jul. 2007.

Swaroop Sahoo received the B.Tech. degree in electrical engineering from Biju Pattnaik University of Technology, Bhubaneswar, India, in 2005, and the M.S. degree in electrical engineering from Colorado State University, Fort Collins, CO, USA, in 2011. He is currently working toward the Ph.D. degree in electrical engineering at Colorado State University.

Xavier Bosch-Lluis received the Master's degree in telecommunication engineering specialized in communications systems, the M.Sc. degree in research on information and communication technologies (MERIT), the Master's degree in electronics engineering, and the Ph.D. degree in department of signal theory and communications from the Universitat Politècnica de Catalunya (UPC), Barcelona, Spain, in 2005, 2007, 2010, and 2011, respectively.

Since April 2011, he has been a Postdoctoral Researcher with the Microwave Systems Laboratory, Electrical and Computer Engineering Department, Colorado State University, Fort Collins, CO, USA. His research interests include developing innovative radiometer systems and retrieval algorithms for passive microwave and millimeter-wave remote sensing.

Steven C. Reising (S'88–M'98–SM'04) received the B.S.E.E. (*magna cum laude*) and M.S.E.E. degrees in electrical engineering from Washington University in St. Louis, Saint Louis, MO, USA, in 1989 and 1991, respectively, and the Ph.D. degree in electrical engineering from Stanford University, Stanford, CA, USA, in 1998.

He is currently a Full Professor in electrical and computer engineering with Colorado State University (CSU), Fort Collins, CO, USA, since July 2011, where he served as an Associate Professor from August 2004 to June 2011. Before joining the CSU faculty in 2004, he served as an Assistant Professor in Electrical and Computer Engineering with the University of Massachusetts Amherst, Amherst, MA, USA, where he received tenure. He served as a Summer Faculty Fellow for three summers in the Remote Sensing Division of the Naval Research Laboratory, Washington, DC, USA. His research interests include remote sensing disciplines, passive microwave and millimeter-wave remote sensing of the oceans, atmosphere, and land; microwave circuits and radiometer systems; lidar systems for sensing of temperature and winds in the middle and upper atmosphere; and atmospheric electrodynamics. He has been the Principal Investigator of more than 12 grants from the National Science Foundation (NSF), NASA, Office of Naval Research (ONR), National Polar-orbiting Operational Environmental Satellite System Integrated Program Office, European Space Agency, and Ball Aerospace and Technologies Corporation.

Dr. Reising serves as the Vice President of Information Resources (2011–present) and formerly as the Vice President of Technical Activities (2008–2010) of the IEEE Geoscience and Remote Sensing Society (GRSS). He has served as an elected member of the IEEE Microwave Theory and Techniques Society (MTT-S) Administrative Committee (AdCom) since January 2014, for which he is currently Technical Coordinating Committee Vice-Chair and Outstanding Chapter Award Co-Chair. He has served as an elected member of the IEEE GRSS AdCom continuously since 2003, after three-year terms as Editor of the GRSS Newsletter (2000–2002), and Associate Editor for University Profiles (1998–2000). He was an Associate Editor of the IEEE TRANSACTIONS ON GEOSCIENCE AND REMOTE SENSING LETTERS (GRSL) from its founding in 2004 to 2013. He has been a Guest Editor of IEEE TRANSACTIONS ON GEOSCIENCE AND REMOTE SENSING (TGRS) for the International Geoscience and Remote Sensing Symposium (IGARSS) 2012 Special Issue published in September 2013, the IGARSS 2008 Special Issue published in November 2009 and the Special Issue on Microwave Radiometry and Remote Sensing Applications published in July 2007. He has served as a Reviewer for TGRS, GRSL, the IEEE TRANSACTIONS ON MICROWAVE THEORY AND TECHNIQUES, *Remote Sensing of Environment*, the *Journal of Atmospheric and Oceanic Technology*, the *Journal of Geophysical Research—Oceans*, *Geophysical Research Letters*, *Marine Geodesy*, *Atmospheric Chemistry and Physics*, the *Journal of Oceanography*, and *Radio Science*. He was the recipient of the NSF CAREER Award (2003–2008) in the areas of physical and mesoscale dynamic meteorology and the ONR Young Investigator Program Award (2000–2003) for passive microwave remote sensing of the oceans. He was awarded the Barbara H. and Joseph I. Goldstein Outstanding Junior Faculty Award in 2004, the Lilly Teaching Fellowship for 2001–2002, and a Young Scientist Award at the URSI General Assembly in Toronto, Canada, in 1999. While at Stanford, he received first place in the United States National Committee (USNC) of URSI Student Paper Competition at the National Radio Science Meeting in Boulder, CO, USA, in 1998. In organizing scientific meetings, he was one of two Technical Program Co-Chairs of the IEEE IGARSS 2008 in Boston, MA, USA, with over 1700 attendees. He served as the General Chair of MicroRad'06, the 9th Specialist Meeting on Microwave Radiometry, held in March 2006 in San Juan, Puerto Rico, with 126 attendees from 15 countries. He was the Local Arrangements Chair for IGARSS 2006 in Denver, with over 1250 attendees. He has been an active participant in each IGARSS Technical Program Committee from 2001 to the present. He serves the URSI as the Chair (2012–2014) and previously as Secretary and Chair-Elect (2009–2011) of its USNC, consisting of 10 scientific commissions focusing on the theory and applications of electromagnetics and radio waves from ultra-low frequencies to Terahertz. He chaired the first three URSI International Student Paper Prize Competitions at the URSI General Assemblies and Scientific Symposia held in Chicago, IL, USA, in 2008; Istanbul, Turkey, in 2011; and Beijing, China, in 2014. Previously, he chaired the annual USNC-URSI Student Paper Prize Competition at the National Radio Science Meeting in Boulder each year from 2004 to 2008 and at the URSI North American Radio Science Meeting in Ottawa, in 2007. In addition, he has served as Technical Program Co-Chair for the USNC-URSI National Radio Science Meetings held each January in Boulder, CO, USA, from 2010 to 2014. He served as the Secretary of USNC-URSI Commission F (2006–2008) and is a member of URSI Commissions F, G, and H, the American Meteorological Society, the American Geophysical Union, Tau Beta Pi, and Eta Kappa Nu.

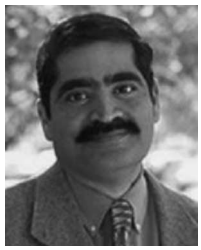

Jothiram Vivekanandan (M'05–SM'10) received the B.E. degree in electronics and communications engineering from the Madurai-Kamaraj University, Madurai, India, the M.Tech. degree in microwave and radar engineering from the Indian Institute of Technology, Kharagpur, India, and the Ph.D. degree in electrical engineering from Colorado State University, Fort Collins, CO, USA, in 1986.

He holds a Senior Scientist appointment in both the Earth Observing Laboratory and the Research Applications Laboratory, National Center for Atmospheric Research (NCAR), Boulder, CO, USA. He led the development of the dual-wavelength system by adding millimeter-wave radar to NCAR's S-band polarization radar (S-Pol). He is currently involved in building airborne cloud radar and provides scientific leadership to lidar remote sensing. He collaborates with a number of research groups toward the development of airborne and ground-based polarization and Doppler weather radar at centimeter wavelengths. He is an Associate Editor of Radio Science. His research interests include interpretation of remote sensing instruments' responses to clouds and precipitation using mathematical models and actual field observations.